Revisited Mechanism of Reaction Between Model Lysine Amino Acid Side Chain and 4-Hydroxynonenal in Different Solvent Environments

Sanja Škulj, Katarina Vazdar, Davor Margetić, Mario Vazdar*

Division of Organic Chemistry and Biochemistry, Rudjer Bošković Institute, Bijenička 54, HR-10000 Zagreb, Croatia

*Corresponding author: e-mail : mario.vazdar@irb.hr

TOC Graphic

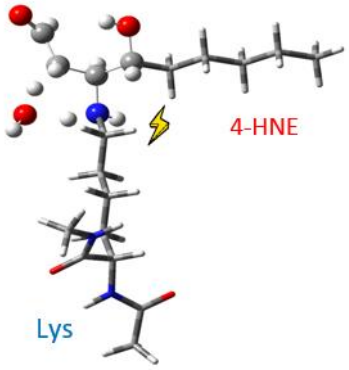

Abstract

We revisit the reaction mechanism of reaction between model lysine side chain and reactive aldehyde 4-hydroxynonenal in different solvents with increasing water content. We show by model organic reactions and qualitative spectrometric analysis that non-polar pyrrole adduct is dominantly formed in non-aqueous solvents dichloromethane and acetonitrile. On the other hand, in aqueous acetonitrile and neat water, other polar products are also isolated including Michael adducts, hemiacetal adducts and pyridinium salt adducts, at the same time decreasing the ratio of non-polar products vs polar products. The experiments are supported by detailed quantum chemical calculations of the reaction mechanism with different computational setups showing that the pyrrole adduct is the most thermodynamically stable product compared to Michael adducts and hemiacetal adducts and also indicating that water molecules released along the reaction pathway are catalyzing reaction steps involving proton transfer. Finally, we also identify the mechanism of the pyridinium salt adduct which is formed only in aqueous solutions.

Introduction

Nucleophilic addition of different amino acids containing amino groups, such as lysine, arginine and histidine towards various reactive aldehydes (RAs) generated during oxidative stress, represents one of the main modifications of proteins in living organisms.[1–4] The most prominent example of reactive aldehydes involved in protein modification is 4-hydroxynonenal (4-HNE, Figure 1)[5,6] which is generated during adenosine triphosphate (ATP) generation[7] in mitochondria in a cascade of peroxidation reactions of polyunsaturated fatty acids located in cellular membranes.[8,9]

One of the most important modifications of proteins involving 4-HNE is related to uncoupling proteins (UCPs) found in inner mitochondrial membranes.[10–14] In particular, modification of UCP2 protein leads to the alteration of protein function causing imbalance in the proton transfer across mitochondrial membranes in turn disturbing the delicate energy balance in the cell.[15] This can trigger various deleterious processes in the living organism and ultimately lead to different dangerous diseases such as diabetes 2, cancer, Parkinson's disease, Alzheimer's disease or atherosclerosis.[10,16–20] Due to the presence of different reactive sites in 4-HNE, nucleophilic addition of amino group towards C=C or C=O double bond (Figure 1), represents a first step in the protein modification. 4-HNE can modify membrane proteins in a number of different ways. The most common ones are formation of Michael adducts and Schiff bases and it is estimated that up to 8% of 4-HNE will react with peptides and proteins in the cellular membrane.[1,21] Proteins which are modified by 4-HNE are usually removed by the cellular proteasome system and low concentrations of modified proteins are normally not harmful.[3,22] However, modified proteins in high concentrations cannot be metabolized completely and severe consequences can occur, causing harmful effects.[21]

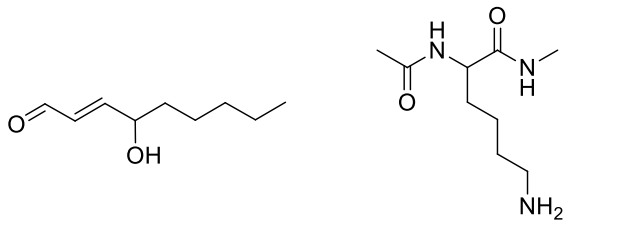

Figure 1. Schematic representation of 4-HNE and the model lysine side chain.

In addition to reactions with proteins, 4-HNE and other RAs can also react with amino groups in phospholipids located in cellular membranes[23–25] as well as DNA and RNA bases.[26,27] In our previous work, we have found that modification of phospholipids increases proton transfer rate upon addition of RAs to model membranes containing UCP2 proteins.[28] Also, we have studied reactivity between phospholipids and 4-HNE as well as its oxidized form 4-oxononenal (4-ONE) in dichloromethane showing that small differences in the initial chemical structure of reactive aldehydes can result in different final reaction products.[29]

To the best of our knowledge, a detailed reaction mechanism involving various reaction pathways of amino acid side chain modification has not been reported to this date. However, there is a number of proposed reaction mechanisms resulting in different 4-HNE adducts reported in the literature, mainly by the group of Sayre,[30–32] but none of them has been accompanied by computational work which would provide a quantitative energetics of the reaction. Moreover, for some of the adducts, such as pyridinium salt adduct also identified in this work, the reaction mechanism has been undetermined to date.[33–37]

Previously, we have studied reactivity of phospholipid amino group towards reactive aldehydes in inert dichloromethane, where influence of the solvent has not been detrimental. In this work, we greatly expand and revisit the present findings focusing instead on the reaction between model lysine amino acid side chain and 4-HNE (Figure 1). We study in full details the reaction mechanism using a combination of quantum-chemical (QM) methods and model experiments in different solvents – non-aqueous dichloromethane and acetonitrile as well as various mixtures of acetonitrile and water. In this way, we aim to study the effect of explicit inclusion of water on the reaction course and the product distribution thus making an additional

step closer to the description of aldehyde reactivity in biologically relevant environment where water role is pivotal.

Results

Experimental detection of adducts

Before going into the mechanistic details of the reaction mechanism itself, we present first the results of LC-MS experiments of reaction between model lysine side chain **R** and 4-HNE. Table 1 lists the experimental product composition after reactions, while Figure 2 presents LC-MS results of reaction mixtures together with the proposed main reaction products.

Table 1. Experimental amounts of adducts of the reaction of **R** with 4-HNE determined by LC chromatography. DCM – dichloromethane, ACN – acetonitrile, ACN10 – acetonitrile with 10 mol% of phosphate buffer, ACN50 – acetonitrile with 50 mol% of phosphate buffer, WAT – phosphate buffer.

Solvent	Amounts (%)
DCM	**R**: 4%, **P3**: 7%, **P4**: 76%.
ACN	**R**: 5%, **P3**: 15%, **P4**: 43%.
ACN10	**R**: 6%, **P1**: 13%, **P2**: 16%, **P3**: 11%, **P4**: 13%.
ACN50	**R**: 11%, **P1**: 15%, **P2**: 21%, **P3**: 8%, **P4**: 15%.
WAT	**R**: 17%, **P1**: 40%, **P2**: 16%, **P3**: 3%, **P4**: 9%.

Analysis of Table 1 and Figure 2 shows that in dichloromethane (DCM) the pyrrole derivative **P4** (76%, at $t \approx 35$ min) was dominantly obtained with small amounts of the proposed double adduct **P3** (7%, at $t \approx 24$ min) and unreacted lysine **R** (4%, at $t \approx 2$ min). Pyrrole derivative was additionally identified by ^{1}H-NMR, ^{13}C-NMR, COSY, HSQC and ESI-MS (Figures S1-S5). Upon going to more polar acetonitrile solvent (ACN), the amount of pyrrole adduct **P4** is decreasing almost by half (43%), while the double adduct **P3** is formed in the larger amount (15%). Interestingly, in non-aqueous systems no formation of more polar adducts was observed. Addition of phosphate

buffer to acetonitrile in the ratio of 9:1 (ACN10) and 1:1 (ACN50) yields additional polar adducts **P1** and **P2**. **P1** presents a mixture of isomers with the mass of Michael adducts or their hemiacetal forms (at $t \approx 5 - 8$ min), while **P2** has the mass of the pyridinium salt adduct (at $t \approx 10$ min). It is important to note that nonpolar adducts **P3** and **P4** are formed in smaller amounts with the increase of water content (Table 1).

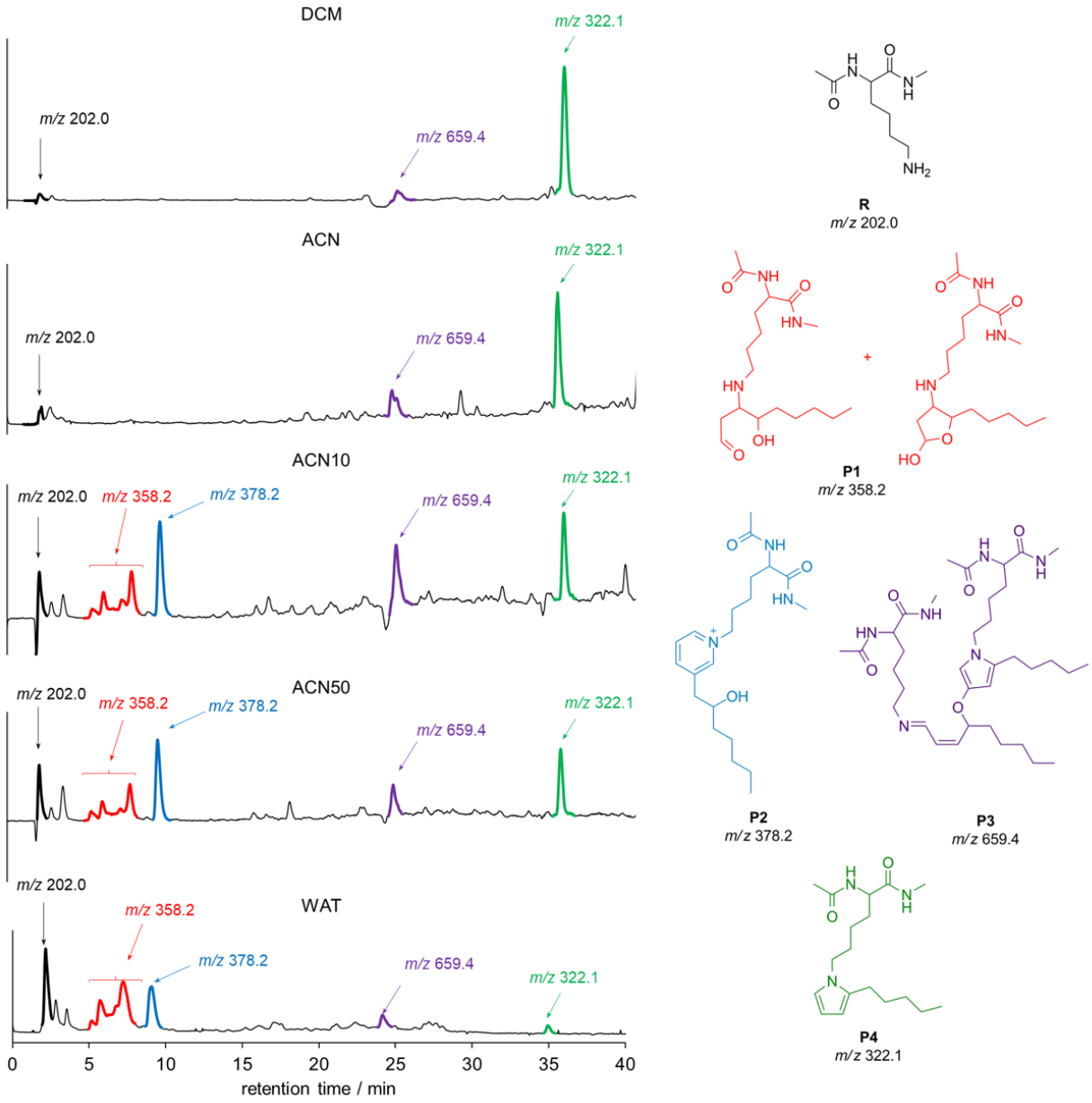

Figure 2. LC-MS analysis of reaction of model lysine side chain **R** with 4-HNE in different solvent systems. DCM – dichloromethane, ACN – acetonitrile, ACN10 – acetonitrile with 10 mol% of phosphate buffer, ACN50 – acetonitrile with 50 mol% of phosphate buffer, WAT – phosphate buffer.

Finally, when only the phosphate buffer is present (WAT), polar adducts **P1** and **P2** are major products (40% and 16%) while other products are formed in significantly lower amounts. The amount of unreacted lysine **R** is the largest in the series, thus indicating that the increase of water content is pushing the reaction towards the reactants. However, the indicated LC/MS yields are not necessarily quantitative since the ionization might not be identical for all of the compounds. Therefore, we decide to check the product distribution in the reaction mixture also with UV/VIS chromatography, using UV light with wavelength of 200 nm. The given procedure has been successfully applied in quantitative analysis of peptides without aromatic side chains.[38] The UV/VIS chromatography analysis is given in Supporting Information (Figure S15), whereas the product yields are given in Table S1. The UV analysis has shown that the amount of the pyrrole derivative **P4** and double adduct **P3** decreases with the amount of water, whereas Michael adducts **P1** and pyrimidine salt **P2** are not visible in neat organic solvents. The calculated yields look qualitatively the same as in the LC/MS experiments, with the exception of lower UV absorbance of Michael adducts in aqueous solutions which is presumably due to different absorption of protonated Michael adducts in water. However, we always see that by increase of water content the ratio of non-polar adducts **P2** and **P4** decreases at the expense of polar adducts **P1** and **P3** and unreacted lysine **R**, which is in qualitative agreement with LC/MS experiments (Figure 2, Table 1).

In order to shed more light to the reaction mechanism involving lysine and 4-HNE and to rationalize the experimental results, we used QM calculations to check in molecular detail all of the reaction steps. Figure S15 shows a complete overview of the postulated reaction mechanism involving reaction between model lysine amino side chain **1** with 4-HNE in the *trans*-configuration **2-t** (the *trans* configuration is kept as produced in cellular membranes) resulting in several possible products of the reaction – Michael and hemiacetal adducts **4** and **5** originating from Michael addition (observed as **P1** in the experiments) as well as the pyrrole derivative **11** (**P4** in the experiments) resulting from cyclization of Schiff bases. In addition, we also reveal all the details of a new reaction mechanism for formation of the pyridinium salt adduct **16** (**P2** in the experiments) and propose a possible mechanism for formation of the double adduct **17** (**P3** in the experiments). Since the reaction mechanism is highly complex and involves a number of reaction

steps, it is partitioned into several parts and we examine all of the reaction steps in the full detail. The calculations are performed at the SMD/MP2/6-311++G(d,p)//B3LYP/6-31G(d) level of theory for two different cases – an inert acetonitrile solvent (ACN) as well as acetonitrile with the inclusion of one explicit water molecule to check for the effect of water on the reaction energetics (this setup will be designed as ACN-W in the further text).

Michael addition and Schiff base formation

The first step of the reaction is the nucleophilic attack of $-NH_2$ group in **1** towards electrophilic carbon atom in the C=C double bond of **2-t**, resulting in the unstable zwitterionic intermediate **3-t** (Figure 3). This step requires 15.2 kcal mol^{-1} in ACN which is almost identical to the free energy barrier of 15.0 kcal mol^{-1} in ACN-W showing that an addition of explicit water does not change the barrier height. After addition, proton transfer from adjacent carbon atom takes place, resulting in the Michael adduct **4** which is more stable than the pre-reactive complex **1 + 2-t** by -7.1 and -10.5 kcal mol^{-1} in DCM and ACN, respectively. In this step, the free energy barrier is by ca. 13 kcal mol^{-1} higher in ACN (24.5 kcal mol^{-1}) as compared to ACN-W (11.6 kcal mol^{-1}) where an explicit water molecule strongly assists the proton transfer.[39] It should be mentioned that further addition of water decreases the free energy barrier for the proton transfer (at the B3LYP/6-31G(d) level of theory this value decreases by additional ca. 4 kcal mol^{-1} for this particular transition state), but the proper characterization of all transition states with two explicit water molecules is very difficult due to a significantly larger number of possible conformers which cannot be properly accounted for in the static *ab-initio* calculations performed in this work.

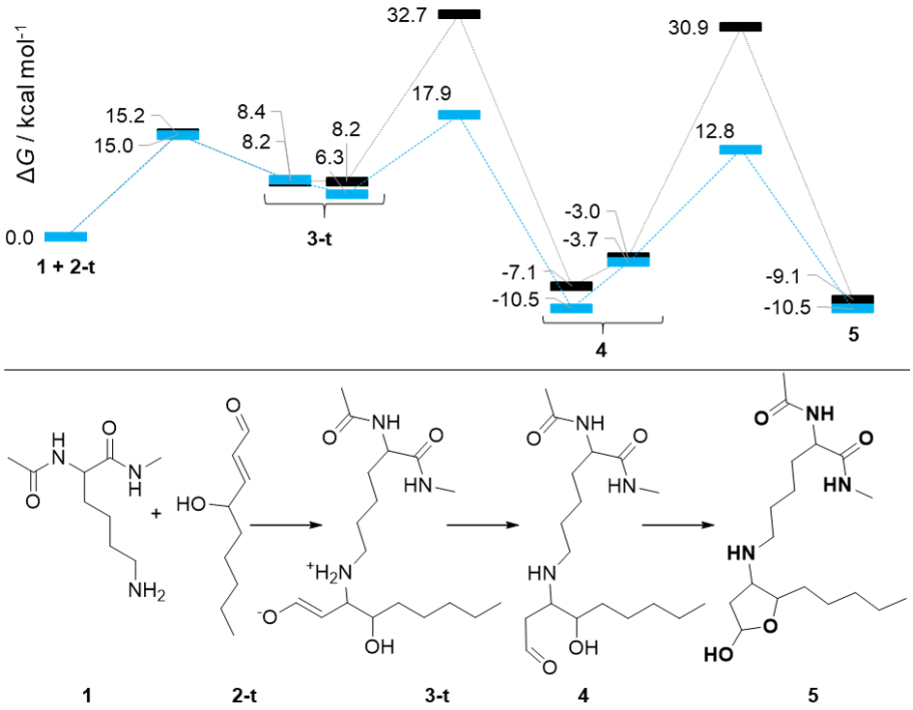

Figure 3. Michael addition of **1** to **2-t** and formation of adducts **4** and **5**. Free energy barriers (in kcal mol^{-1}) are calculated at the SMD/MP2/6-311++G(d,p)//B3LYP/6-31G(d) level of theory in ACN (black color) and ACN-W (blue color). Conformational changes leading to the next reaction step within the same molecule are indicated above the curly bracket.

After formation of **4**, the reaction proceeds further with an additional proton transfer and a cyclization step, yielding the final hemiacetal adduct **5**, which is by 2 kcal mol^{-1} more stable than **4** in ACN (-7.1 and -9.1 kcal mol^{-1} *vs*. reactants), and of equal stability in ACN-W (-10.5 kcal mol^{-1} *vs*. reactants). Free energy barriers for the reaction are 34.6 kcal mol^{-1} in ACN and 16.5 kcal mol^{-1} in ACN-W. However, the question of existence of Michael adducts **4** and/or hemiacetal adduct **5** is quite controversial. In particular, Sayre and coworkers have not been able to isolate Michael adducts and corresponding hemiacetal derivatives after Michael addition of primary amine with 4-HNE due to their instability upon isolation in mixed aqueous-organic solvents.[31,32] On the other hand, Petersen and coworkers have characterized Michael adducts after addition of 4-HNE to various model peptides in aqueous sodium buffer using ESI-MS,[40] as shown here as well. In our case, we see that Michael derivative **4** and/or hemiacetal derivative **5** are indeed isolated in ESI-MS only if aqueous solvent mixture is present (product **P1**, table 1), in contrast to non-aqueous

dichloromethane and acetonitrile. However, we were also not able to isolate the Michael product **P1** directly using column chromatography on silica gel of pure products (in turn preventing NMR analysis) and we believe that this is related to the higher degree of the reaction reversibility on acidic silica gel in comparison to less acidic conditions used in LC-MS experiments. We see from QM calculations that the stability of **4** and **5** is identical in ACN-W systems indicating that they can both exist in the equilibrium in the reaction mixture. This is in agreement with LC-MS experimental results in WAT where several peaks of **P1** adduct with the same mass (which can belong either to Michael adducts or hemiacetals) are found in the broader elution range (t = 5 – 8 min) in contrast to single peaks for other adducts (Figure 2).

After formation of Michael adducts **4**, the reaction can proceed further along a different route (Figure S16). This scenario does not lead to the formation of **5**, but instead leads back to the reactant **1** and 4-HNE in the *cis* conformation of the pre-reactive complex **1 + 2-c**. (Figure 4). The free energy barriers for reverse Michael addition are higher as compared to the reaction involving **2-t**, and the pre-reactive complex **1 + 2-c** is less stable by 15.0 and 9.9 kcal mol^{-1} in ACN and ACN-W *vs.* pre-reactive complex **1 + 2-t**. Since *cis-trans* isomerization of **2-t** is not taking place at 40 °C (reaction temperature of our experiments),[41] this additional reaction step actually enables further cyclization to the pyrrole derivative due to optimal arrangement of double bonds (Figure 4). The catalytic behavior of primary amines and their role as catalysts via addition and elimination in *cis-trans* isomerization is widely recognized in the literature.[42,43] Since pyrrole derivative is a dominant product in DCM and ACN and also relevant product in the other solvents, the addition/elimination catalytic step can explain why Michael adduct **4** and/or hemiacetal derivative **5** was not detected (albeit thermodynamically stable) in favor of even more thermodynamically stable pyrrole adduct (*vide infra*) in non-aqueous solvent mixtures.

At this point, we should note that the Michael addition reactions are energetically very demanding involving almost prohibitively high free energy barriers above 30 kcal mol^{-1} in ACN when no water molecules are included (Figures 3 and 4, black color). When only one catalytic water molecule is included in the calculations, this step becomes energetically feasible resulting in free energy barriers of around 20 kcal mol^{-1} (Figures 3 and 4, blue color).

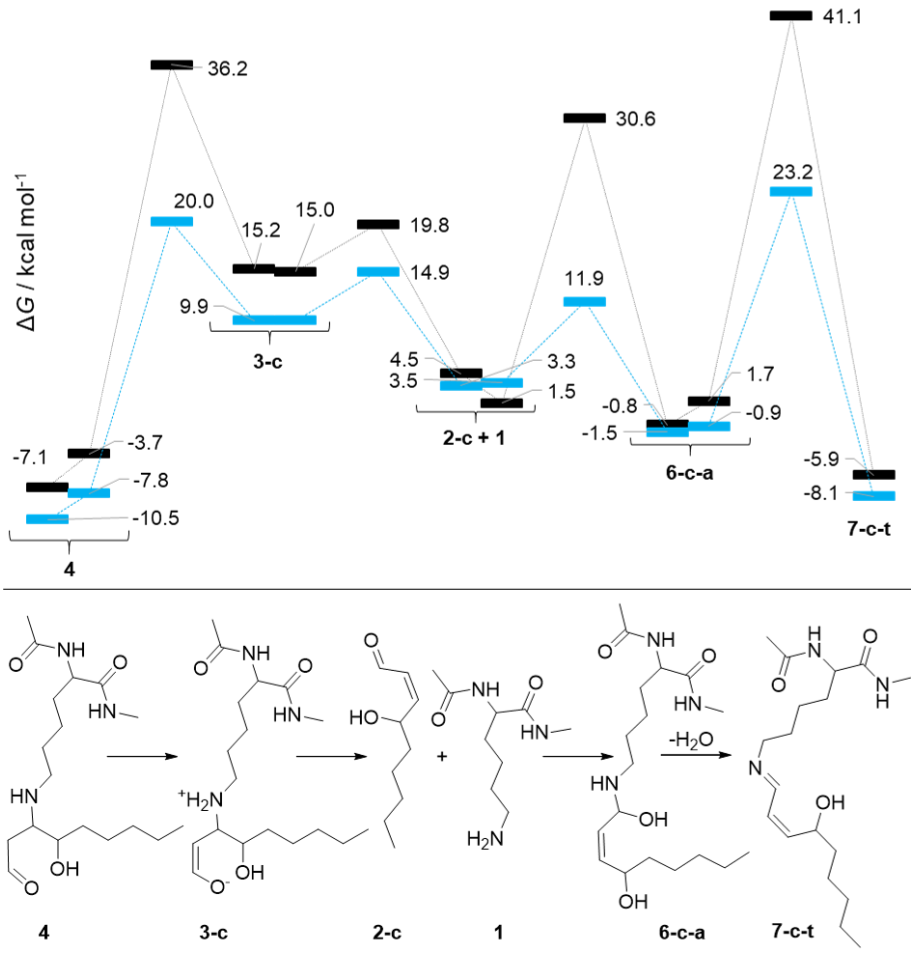

Figure 4. Schiff base **7-c-t** formation from Michael adduct **4**. Free energy barriers (in kcal mol^{-1}) are calculated at the SMD/MP2/6-311++G(d,p)//B3LYP/6-31G(d) level of theory in ACN (black color) and ACN-W (blue color). Conformational changes leading to the next reaction step within the same molecule are indicated above the curly bracket.

After *cis-trans* conformational change of **2-t** to **2-c**, the pre-reactive complex **1 + 2-c** can react *via* proton transfer where the hydroxynonenal fragment is oriented in the *anti*-fashion vs. the lysine fragment (See Supporting Information for geometries) which costs 29.1 kcal mol^{-1} in ACN and 8.6 kcal mol^{-1} in ACN-W system. A subsequent proton transfer and water molecule loss results in the Schiff base **7-c-t** where C=C double bond is in *cis* configuration and N=C double bond is in *trans* configuration, with the barriers of 39.4 and 24.1 kcal mol^{-1} in ACN and ACN-W. Importantly, during formation of the Schiff base adduct one water molecule is released which can act catalytically

significantly reducing free energy barriers involving proton transfer in the further course of the reaction.

We should mention that additional mechanistic routes are also possible after reaction of **1** + **2-t**, where Schiff bases **7-t-c** and **7-t-t** are formed (Figures S16-S18). Despite their relative thermodynamic stability, we did not isolate any of the Schiff bases experimentally suggesting that **7-t-c** is transformed back to reactants resulting in the formation of the more stable pyrrole adduct, whereas **7-t-t** can transform further to **8** and subsequent pyrrole adducts (see below). A similar situation also holds for reaction between **1** and **2-c** where **7-c-c** is formed (Figure S16 and S19) and **7-c-c** can further transform to relatively stable furan derivative **12** (also suggested by Sayre and coworkers[30]) but it was also not isolated in our system.

Pyrrole and double adduct formation

In the previous section, we described the reaction mechanism leading to the formation of Schiff base adducts. Since Schiff bases were not detected in any of our experimental systems (Table 1), **7-c-t** serves as a starting reagent for formation of the thermodynamically very stable pyrrole adduct **11** (Figure 5)[29,32] which was detected in all solvents in different ratios as product **P4** (Table 1, Table S1, Figure 2, Figure S15). A necessary condition for cyclization of the Schiff bases is a geometric prerequisite that N=C double bond is in the *trans* configuration thus allowing efficient proton transfer to the adduct **8** which is satisfied in the adduct **7-c-t**. The energetic cost for this step is 25.1 and 27.7 kcal mol^{-1} in ACN and ACN-W, where we see that addition of water molecule does not lead to the reduction of the free energy barrier due to the spatial restrictions and inability of water molecule to optimally insert and assist in the proton transfer. In the next step, an additional proton transfer is required leading to the adduct **9** with barriers of 50.5 and 33.0 kcal mol^{-1} in ACN and ACN-W. We see here that the energy cost of proton transfer is inhibitive in ACN but feasible when catalytic water, released in previous reaction steps, is present. The penultimate reaction step involves cyclization of the five-membered ring to the adduct **10** with free energy barriers of 31.6 and 18.7 kcal mol^{-1} in ACN and ACN-W. Finally, water molecule loss (with barriers of 34.5 and 23.0 kcal mol^{-1} in ACN and ACN-W) in the adduct **10** leads to the pyrrole adduct **11** which is thermodynamically the most stable adduct, being 41.3 and 43.0 kcal mol^{-1}

more stable than the starting pre-reactive complex **1 + 2-t**. The Figure 5 also shows that all of the adducts in this part of reaction mechanism are getting stabilized along the route *vs.* initial reactants, as indicated by stabilization free energies of **7-c-t**, **8**, **9** and **10** of -5.9, -10.0, -16.3 and -15.8 kcal mol^{-1} in ACN, and -8.1, -11.4, -17.2 and -18.3 kcal mol^{-1} in ACN-W, respectively.

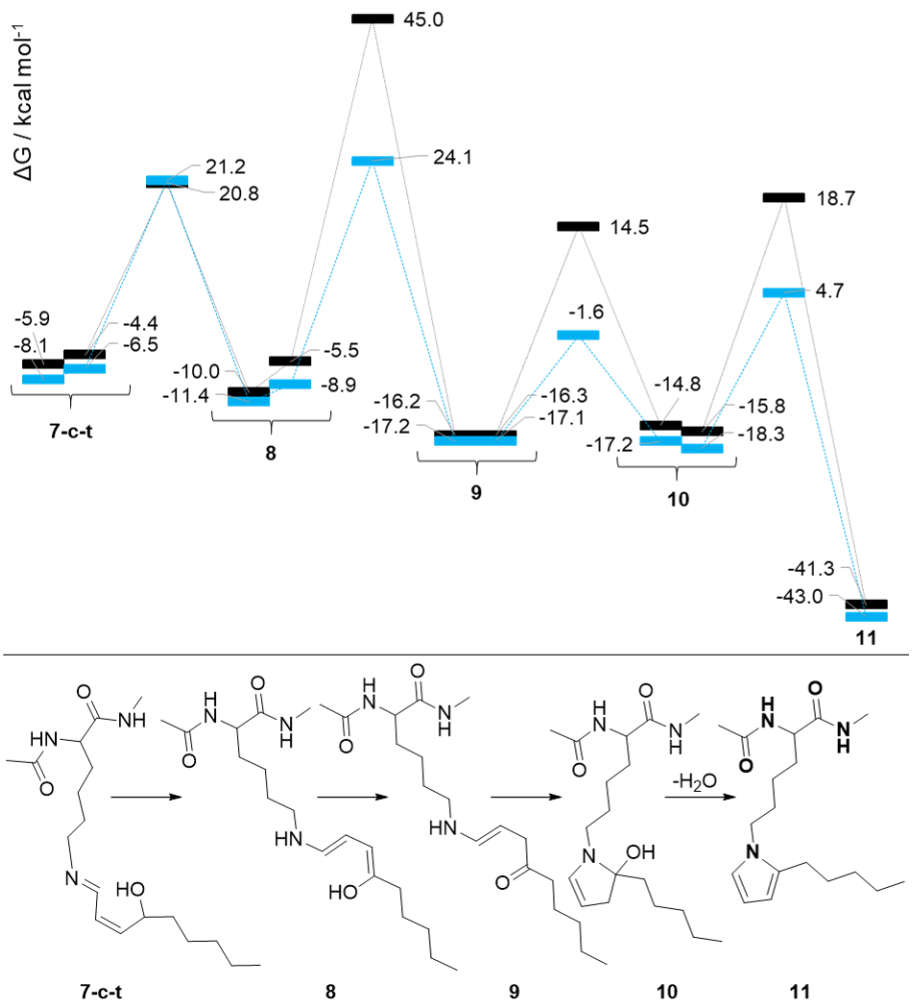

Figure 5. Pyrrole adduct **11** formation from Schiff base **7-c-t**. Free energy barriers (in kcal mol^{-1}) are calculated at the SMD/MP2/6-311++G(d,p)//B3LYP/6-31G(d) level of theory in ACN (black color) and ACN-W (blue color). Conformational changes leading to the next reaction step within the same molecule are indicated above the curly bracket.

We propose here also the mechanism of the double adduct **P3** formation which was observed in all systems studied (Table 1). The formation of the double adduct is closely related to the formation of the pyrrole adduct (Table 1) suggesting that the pyrrole derivative is formed first. Therefore, we chose the pyrrole derivative **11** as the starting point for formation of the double adduct which reacts with the Schiff base adduct **7-c-t**, followed by autooxidation of the newly formed pyrrole ring by triplet molecular oxygen (Figure 6).[44] This reaction is an example of

covalent protein crosslinking[45] which is one of the main modifications of proteins.[3,30] In our experimental setup, we were not able to detect other double adducts in sufficient yield. Unfortunately, due to high molecular mass of the final double adducts and involved triplet spin state, we are not able to present reliable energy calculations at the MP2 level for the double adduct **17** due to too high computational burden.

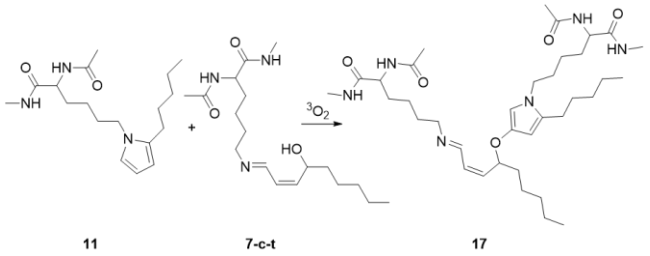

Figure 6. Proposed reaction mechanism for double adduct formation **17** from the Schiff base **7-c-t** and the pyrrole derivative **11**.

Pyridine salt adduct formation

In addition to the Michael adducts/hemiacetals mixture **P1** and the pyrrole adduct **P4**, which are usual products of reaction between lysine and 4-HNE, we also detected a significant amount of pyridinium salt adduct **P3** in aqueous solvent mixtures (Table 1). As mentioned previously, this adduct has been observed in the experiments[33–37] but the details of the mechanism have not been fully understood. In the Figure 7, we present a detailed mechanism how pyridinium salt adduct forms in aqueous solutions.

Since pyridinium salt adducts were not detected in DCM and ACN (Table 1, Table S1), we start the mechanism assuming the reaction between protonated aldehyde **2-t**$^+$ with the Schiff base adduct **7-c-t** in ACN-W system only. Protonation of aldehyde is energetically disfavored step in water (see Computational Details), but it is necessary to obtain the final protonated pyridinium salt. After protonation of **2-t** and nucleophilic addition to Schiff base **7-c-t**, the adduct **13** is formed. The free energy barrier for this reaction step is only 2.0 kcal mol^{-1}. Subsequently, the adduct **13** cyclizes to the adduct **14** with the free energy barrier of 20.0 kcal mol^{-1}. After conformational rearrangement of the adduct **14**, the aldehyde fragment is lost which leads to the dihydropyridinium salt **15** with free energy barrier of 32.2 kcal mol^{-1}. A final step, aromatization

and loss of water which cost 26.8 kcal mol^{-1}, leads to the final thermodynamically very stable pyridinium salt product **16** which is stabilized by -68.3 kcal mol^{-1} vs. initial protonated pre-reactive complex **2t$^+$ + 7-c-t**. We should mention that this adduct has a different structure and –OH group at the alkyl tail is in β position *vs.* aromatic ring compared to the adducts suggested in the literature where –OH group is in the α-position.[35,36]

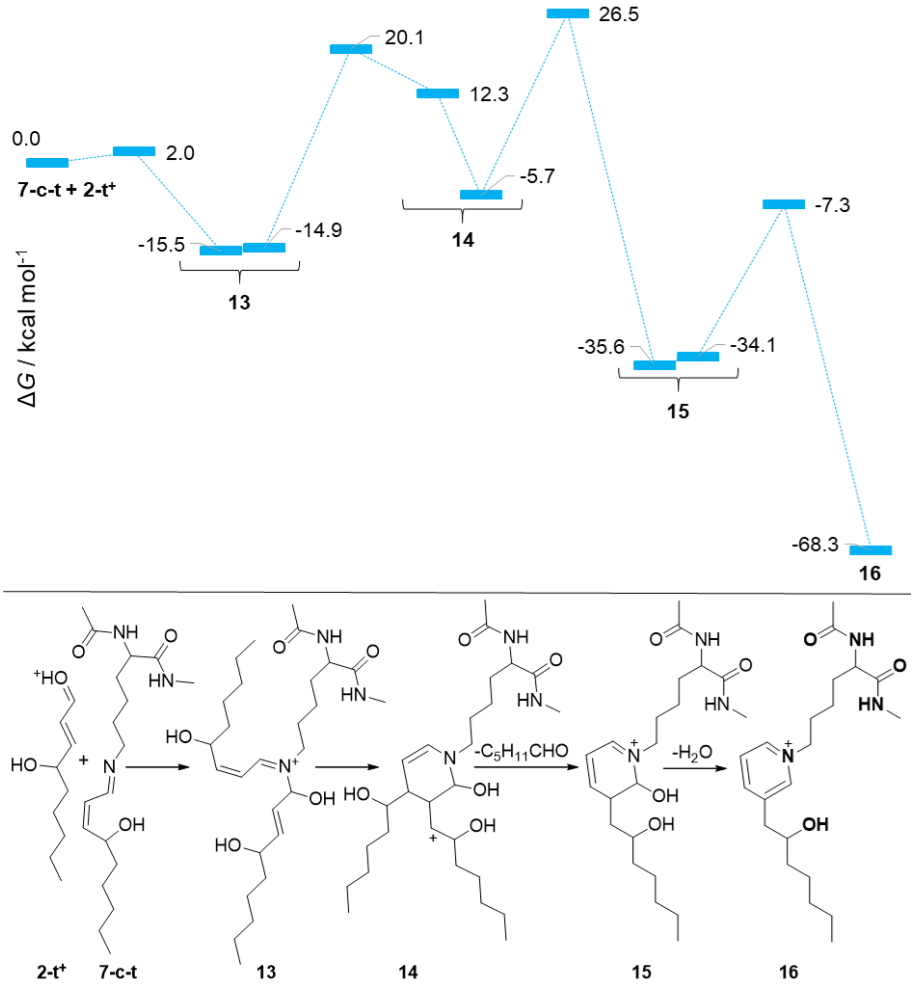

Figure 7. Pyridinium salt adduct **16** formation from Schiff base **7-c-t** and protonated 4-HNE. Free energy barriers (in kcal mol^{-1}) are calculated at the SMD/MP2/6-311++G(d,p)//B3LYP/6-31G(d) level of theory in ACN-W (blue color). Conformational changes leading to the next reaction step within the same molecule are indicated above the curly bracket.

Discussion and conclusions

In this work we revisited the reaction mechanism between the lysine side chain and 4-hydroxynonenal with the help of model organic reactions in different solvents (dichloromethane – DCM, acetonitrile – ACN, acetonitrile with 10% of water – ACN10, acetonitrile with 50% of water – ACN50 and water – WAT) accompanied with LC-MS and NMR spectroscopy. We checked the energetics of the reaction by QM calculations at SMD/MP2/6-311++G(d,p)//B3LYP/6-31G(d) level of theory in two model solvents – acetonitrile (ACN) and acetonitrile with the catalytic water molecule (ACN-W).

By NMR,ESI-MS and UV/VIS analysis, we showed that the main product in DCM and ACN is the pyrrole adduct **P4** with a significant contribution of the double adduct **P3**. Adding water to the acetonitrile increases the amount of the polar adducts **P1** (which is a mixture of Michael adducts and derived hemiacetals) together with **P2** which is identified as the pyridinium salt adduct. At the same time, the amount of non-polar pyrrole adducts **P4** decreases significantly as well as the double adduct **P3**. Unfortunately, it was not possible to quantitatively determine the exact amount of products with LC/MS and UV/VIS spectroscopy methods used in this work. Nevertheless, the presented experimental data strongly indicates that the ratio of nonpolar adduct **P3** and **P4** versus polar adducts **P1** and **P2** decreases when water excess increases.These results are connected to QM calculations which have identified all of the elementary steps of the reactions yielding products **4** and **5** (**P1** in experiments), **16** (**P2** in experiments) and **11** (**P4** in experiments) and nicely agree with the experimental results showing qualitative trends in the production distribution, depending on the solvent. In addition, the energetics of the reaction show several important roles of water in the reaction pathway. First, in almost all of the reaction steps leading to **4**/**5** and **16** (Figures 3-5 and 7) involving proton transfer the free energy barriers for the transfer are significantly reduced, going from prohibitively large 40 – 50 kcal mol^{-1} in ACN systems to 20 – 30 kcal mol^{-1} in ACN-W systems. Here we underpin the catalytic effect of water molecule which is released along the reaction pathway upon conversion of the carbinolamines **6-c-a** to the Schiff bases **7-c-t** and cyclization to the pyrrole adduct **11** which is essential for reaction to even proceed in experiments with non-aqueous solvents (DCM and ACN) where water is not present. This leads to the second surprising role of water, which is evident in aqueous systems

with abundance of water which pushes the reaction equilibrium towards reactants. Since pyrrole cyclization results in the water molecule loss[29,32] this is a nice example of the Le Chatelier's principle,[7] which is operative when water excess is present. In other words, although water is essential for the kinetics of the reaction, water excess has the opposing effect upon the formation of otherwise thermodynamically very stable pyrrole adduct **P4** and the double adduct **P3**. Finally, only in aqueous systems we see the formation of the pyridinium salt **P2** where water participates in the protonation of 4-HNE (Figure 7) and we propose the reaction mechanism for its formation.

Taken together, we show that the distribution of reaction products is different depending mainly on the water excess which can accelerate/decelerate different reactions as well as stabilize/destabilize different reaction products. This has been already noticed in the literature where it has been shown that non-polar Schiff bases and pyrrole derivatives are usually formed in hydrophobic environments, such as organic solvents[24,28,29,35] whereas in the aqueous systems only Michael adducts were isolated.[2,31,40]

In this work we further analyze the presence of water in more details showing that reaction with aldehydes is impossible without the water catalytic effect, but on other side thermodynamically very stable products are not formed due to the water excess. Since the environment in the cellular membranes where membrane proteins are attached or immersed is highly heterogeneous and lysine side chains can easily fluctuate in the membrane environment being constantly exposed to the different local microenvironments,[46–48] it is especially challenging to predict how reactions of proteins or lipids with various deleterious compounds generated during oxidative stress take place, since different amount of water can lead to different reaction products and in turn change biophysical properties of membranes.[28] A similar behavior has also been observed in the modelling of emulsion polymerization, where polymerization kinetics strongly depends on the balance of water excess and hydrophobicity.[49] Besides reactions of proteins and lipids with reactive aldehydes during oxidative stress,[8,9] reactive oxygen species (such as superoxide radical and hydroxyl radical) can also directly react with lipids and proteins during neurodegeneration which is also directly related to membrane heterogeneity and hydration.[50] This work presents an important step towards clarification of reaction mechanisms

relevant for heterogeneous biological environment and oxidative stress which continuously occurs in living cells. Also, it sets the foundation for future efforts which will address chemical reactivity of more complicated peptides/proteins with reactive aldehydes in realistic biological membranes utilizing various QM/MM methods. [51,52]

Experimental Details

General

All reactions were performed under argon atmosphere. Model lysine side chain Ac-Lys-NMe (R) was dissolved in the solvent of interest (DCM – dichloromethane, ACN – acetonitrile, ACN10 – acetonitrile with 10 mol% of phosphate buffer, ACN50 – acetonitrile with 50 mol% of phosphate buffer, WAT – phosphate buffer). 4-HNE was added and stirred at 40 ^{o}C for 18 h. Commercially available reagents were used without further purification. 4-HNE and Ac-Lys-NMe were prepared according to known literature procedures.[53–55] The phosphate buffer solution of pH 7.4 was prepared by dissolving disodium hydrogen phosphate (Na_2HPO_4, 10.9 g) and sodium dihydrogen phosphate (NaH_2PO_4, 2.7 g) in distilled, deionized water (1000 mL) to make a 0.1 M solution. Column chromatography on silica gel 60, 70-230 mesh, 60 Å (E. Merck, Darmstadt, Germany) was performed at RT. Thin layer chromatography was carried out on TLC aluminium sheets, 20x20 cm, silica gel 60 F254. Liquid chromatography-mass spectrometry (LC-MS) and UV/VIS chromatography analysis were performed on an Agilent 1200 LC-MS System equipped with an Agilent Diode Array Detector and an Agilent 6410 Triple Quadrupole Mass Spectrometer Detector applying electrospray ionization (ESI) (Agilent Technologies Inc., Wilmington, DE, USA) in positive and negative mode. UV/VIS chromatography was performed in the range of wavelengths of 190 – 400 nm, whereas the wavelength of 200 nm was selected for the analysis.[38] The NMR spectra (in $CDCl_3$ at RT) were measured on a Bruker AV 600 spectrometer (Bruker BioSpin GmbH., Rheinstetten, Germany).

Synthesis of pyrrole adduct

Ac-Lys-NMe (25 mg, 0.124 mmol, 1.0 equiv) was dissolved in 1.2 mL of dry dichloromethane. 4-HNE (4-hydroxy-2-nonenal, 20.0 mg, 0.124 mmol, 1.0 equiv) was added and the reaction mixture

stirred at 40 ^{o}C for 24 h. The reaction mixture was evaporated to dryness and the product **P4** was purified by silica gel column chromatography using petroleum ether and EtOAc (1:1) as eluent. 24 mg (61%) of product **P4** was obtained as brown solid.

^{1}H NMR (600 MHz, MeOD) 6.59 (dd, *J* = 2.7, 1.8 Hz, 1H, 1H-pyrrole), 5.97-5.98 (m, 1H, pyrrole), 5.80-5.81 (m, 1H, pyrrole) 4.28 (dd, *J* = 8.9, 5.4 Hz, 1H, C<u>H</u>CONHCH$_3$), 3.86 (t, *J* = 7.1 Hz, 2H, CH$_2$N-pyrrole), 2.76 (s, 3H, NHC<u>H</u>$_3$), 2.54-2.58 (m, 2H, CH$_2$-pyrrole), 2.02 (s, 3H, COCH$_3$), 1.78-1.76 (m, 2H, CH$_2$-Lys), 1.71-1.77 (m, 2H, CH$_2$-Lys), 1.62-1.70 (m, 4H, CH$_2$-Lys+CH$_2$-HNE), 1.30-1.46 (m, 4H, 2xCH$_2$-HNE), 0.94-0.99 (m, 3H, CH$_3$-HNE). ^{13}C{H} NMR (151 MHz, MeOD) 173.5 (<u>C</u>ONHCH$_3$), 171.9 (COCH$_3$), 132.5 (C, pyrrole), 119.3 (CH, pyrrole), 106.0 (CH, pyrrole), 104.8 (CH-pyrrole), 53.3 (<u>C</u>HCONHCH$_3$), 45.5 (CH$_2$N-pyrrole), 31.4 (CH$_2$-Lys), 31.3 (CH$_2$-Lys), 30.7 (CH$_2$-HNE), 28.7 (CH$_2$-HNE), 25.7 (NH<u>C</u>H$_3$), 24.9 (CH$_2$-Lys), 22.7 (CH$_2$-HNE), 22.2 (CH$_2$-HNE), 21.1 (COCH$_3$), 13.0 (CH$_3$-HNE). **P4:** LRMS (ESI) m/z: [M-H]$^{-}$ Calcd. for $C_{18}H_{31}N_3O_2$ 320.2; Found 320.1. [M+H]$^{+}$ Calcd. for $C_{18}H_{31}N_3O_2$ 322.2; Found 322.1.

LC-MS experiments

Dichloromethane (DCM)

Ac-Lys-NMe (13 mg, 0.064 mmol, 1.0 equiv) was dissolved in 0.65 mL of dry dichloromethane. 4-HNE (4-hydroxy-2-nonenal, 10.0 mg, 0.064 mmol, 1.0 equiv) was added and the reaction mixture stirred at 40 ^{o}C for 24 h. The reaction mixture was evaporated to dryness and analyzed by LC-MS. Experimental yields of reaction determined by LC – **R**: 4%, **P3**: 7%, **P4**: 76%.

Acetonitrile (ACN)

Ac-Lys-NMe (13 mg, 0.064 mmol, 1.0 equiv) was dissolved in 0.65 mL of dry acetonitrile. 4-HNE (4-hydroxy-2-nonenal, 10.0 mg, 0.064 mmol, 1.0 equiv) was added and the reaction mixture stirred at 40 ^{o}C for 24 h. The reaction mixture was evaporated to dryness and analyzed by LC-MS. Experimental yields of reaction determined by LC – **R**: 5%, **P3**: 15%, **P4**: 43%.

Acetonitrile:phosphate buffer = 9:1 mixture (ACN10)

Ac-Lys-NMe (13 mg, 0.064 mmol, 1.0 equiv) was dissolved in 0.65 mL of acetonitrile: phosphate buffer = 9:1 mixture. 4-HNE (4-hydroxy-2-nonenal, 10.0 mg, 0.064 mmol, 1.0 equiv) was added

and the reaction mixture stirred at 40 ^{o}C for 24 h. The reaction mixture was evaporated to dryness and analyzed by LC-MS. Experimental yields of reaction determined by LC – **R**: 6%, **P1**: 13%, **P2**: 16%, **P3**: 11%, **P4**: 13%.

In acetonitrile:phosphate buffer = 1:1 mixture (ACN50)

Ac-Lys-NMe (13 mg, 0.064 mmol, 1.0 equiv) was dissolved in 0.65 mL of acetonitrile: phosphate buffer = 1:1 mixture. HNE (4-hydroxy-2-nonenal, 10.0 mg, 0.064 mmol, 1.0 equiv) was added and the reaction mixture stirred at 40 ^{o}C for 24 h. The reaction mixture was evaporated to dryness and analyzed by LC-MS. Experimental yields of reaction determined by LC – **R**: 11%, **P1**: 15%, **P2**: 21%, **P3**: 8%, **P4**: 15%.

Phosphate buffer (WAT)

Ac-Lys-NMe (13 mg, 0.064 mmol, 1.0 equiv) was dissolved in 0.65 mL phosphate buffer. 4-HNE (4-hydroxy-2-nonenal, 10.0 mg, 0.064 mmol, 1.0 equiv) was added and the reaction mixture stirred at 40 ^{o}C for 24 h. The reaction mixture was evaporated to dryness and analyzed by LC-MS. Experimental yields of reaction determined by LC – **R**: 17%, **P1**: 40%, **P2**: 16%, **P3**: 3%, **P4**: 9%.

Computational Details

Quantum chemical calculations of reaction mechanism of reaction between model lysine side chain and 4-hydroxynonenal were performed in polar aprotic solvent acetonitrile (ε= 35.7) using SMD solvation model[56] at 298 K and 1 bar (ACN setup). Calculations in acetonitrile were performed with one additional explicit water molecule (ACN-W setup). Despite some limitations of polarizable continuum models, such as inability for proper accounting of entropy effects and appropriate thermal averaging, we believe that use of implicit solvent models represents a good compromise for the systems of interest.[57,58] All calculations were obtained using SMD/MP2/6-311++G(d,p)//B3LYP/6-31G(d) level of theory,[59,60] *i.e.* geometry optimizations were calculated at the SMD/B3LYP/6-31G(d) level of theory followed by MP2 single-point calculations on the optimized structures at the SMD/MP2/6-311++G(d,p) level of theory.[61,62] Stationary points, minima and transition states on the potential energy surface were identified by vibrational

analysis. Transition state structures were verified by the presence of one negative eigenvalue, reaction path following by the Intrinsic Reaction Coordinate (IRC) analysis[63] and by inspecting the displacement along the vibrational mode corresponding to the imaginary frequency. Gibbs free energies were calculated as a sum of single-point electronic energy and thermal correction to Gibbs free energy. All quantum chemical computations have been performed using Gaussian09 suite of codes.[64] In non-aqueous solutions, amino group is not protonated and reaction can proceed without an extra energy cost. However, in aqueous solutions, amino group is protonated and free energy of deprotonation will depend on the pH of solution. Assuming pH of phosphate buffer solutions of 7.4 (see Experimental Details) and pK_a of lysine in water of 10.3 we can calculate the deprotonation cost of lysine by using relationship[65] $\Delta G = 2.303RT(pK_a - pH)$ at 40 °C, which equals 4.2 kcal mol^{-1}. In the same token, we calculated the protonation energy of aldehyde **2-t** assuming its pK_a value in water of 13.3, which equals 8.5 kcal mol^{-1}. We should bear in mind that this costs are only estimates and will be valid only in neat aqueous solutions, whereas in mixed acetonitrile-water solutions these values are different, depending on the ratio of non-aqueous solvent and pK_a values of solutes in the given solvent mixture. In order to easily track the reaction mechanism presented here, we will not explicitly add the protonation/deprotonation free energy to the calculated values, but we are aware of this additional energy cost.

Supporting Information

General data and synthesis of adducts. NMR and MS analysis of pyrrole adduct **P4** (Figures S1-S5), reaction of 4-HNE and Lys in different solvents and LC-MS analysis of reaction mixtures (Figures S6-S10), fragmentation spectra of products **P1**-**P4** (Figures S11-S14). UV/VIS chromatography (Figure S15) and product yields (Table S1). Scheme of the reaction mechanism (Figure S16), energy diagrams (Figures S17-S19), calculated free energies of the compounds (Table S2) and Cartesian coordinates optimized at the B3LYP/6-31G(d) level of theory in ACN and ACN-W systems (Table S3). This material is available free of charge via the Internet at http://pubs.acs.org.

Acknowledgments

This study was supported by Croatian Science Foundation, project no. UIP-2014-09-6090. The computational part of the research was performed using the resources of computer cluster Isabella based in SRCE – University of Zagreb University Computing Center. We also thank Dr. Ivanka Jerić and Dr. Lidija Brkljačić for the instrumental support.

References

(1) Schaur, R. J. Basic Aspects of the Biochemical Reactivity of 4-Hydroxynonenal. *Mol. Aspects Med.* **2003**, *24* (4–5), 149–159.

(2) Petersen, D. R.; Doorn, J. A. Reactions of 4-Hydroxynonenal with Proteins and Cellular Targets. *Free Radic. Biol. Med.* **2004**, *37* (7), 937–945.

(3) Grune, T.; Davies, K. J. A. The Proteasomal System and HNE-Modified Proteins. *Mol. Aspects Med.* **2003**, *24* (4–5), 195–204.

(4) Žarković, N.; Čipak, A.; Jaganjac, M.; Borović, S.; Žarković, K. Pathophysiological Relevance of Aldehydic Protein Modifications. *Journal of Proteomics*. 2013, pp 239–247.

(5) Esterbauer, H.; Schaur, R. J.; Zollner, H. Chemistry and Biochemistry of 4-Hydroxynonenal, Malonaldehyde and Related Aldehydes. *Free Radic. Biol. Med.* **1991**, *11* (1), 81–128.

(6) Poli, G.; Schaur, R. J.; Siems, W. G.; Leonarduzzi, G. 4-Hydroxynonenal: A Membrane Lipid Oxidation Product of Medicinal Interest. *Med. Res. Rev.* **2008**, *28* (4), 569–631.

(7) Berg, J. M.; Tymoczko, J. L.; Stryer, L. *Biochemistry*; W H Freeman: New York, 2002.

(8) Yin, H.; Xu, L.; Porter, N. A. Free Radical Lipid Peroxidation: Mechanisms and Analysis. *Chem. Rev.* **2011**, *111* (10), 5944–5972.

(9) Catala, A. Lipid Peroxidation of Membrane Phospholipids Generates Hydroxy-Alkenals and Oxidized Phospholipids Active in Physiological and/or Pathological Conditions. *Chem. Phys. Lipids* **2009**, *157* (1), 1–11.

(10) Brand, M. D.; Esteves, T. C. Physiological Functions of the Mitochondrial Uncoupling Proteins UCP2 and UCP3. *Cell Metab.* **2005**, *2* (2), 85–93.

(11) Bertholet, A. M.; Kirichok, Y. UCP1: A Transporter for H+ and Fatty Acid Anions. *Biochimie*. 2017, pp 28–34.

(12) Ricquier, D.; Bouillaud, F. The Uncoupling Protein Homologues: UCP1, UCP2, UCP3, StUCP and AtUCP. *Biochem. J.* **2000**, *345* (2), 161–179.

(13) Krauss, S.; Zhang, C. Y.; Lowell, B. B. The Mitochondrial Uncoupling-Protein Homologues. *Nat. Rev. Mol. Cell Biol.* **2005**, *6* (3), 248–261.

(14) Smith, A. M. O.; Ratcliffe, R. G.; Sweetlove, L. J. Activation and Function of Mitochondrial

Uncoupling Protein in Plants. *J. Biol. Chem.* **2004**, *279* (50), 51944–51952.

(15) Boss, O.; Hagen, T.; Lowell, B. B. Uncoupling Proteins 2 and 3: Potential Regulators of Mitochondrial Energy Metabolism. *Diabetes* **2000**, *49* (2), 143–156.

(16) Lowell, B. B.; Shulman, G. I. Mitochondrial Dysfunction and Type 2 Diabetes. *Science* **2005**, *307* (5708), 384–387.

(17) Zhang, C. Y.; Baffy, G.; Perret, P.; Krauss, S.; Peroni, O.; Grujic, D.; Hagen, T.; Vidal-Puig, A. J.; Boss, O.; Kim, Y. B.; Zheng, X. X.; Wheeler, M. B.; Shulman, G. I.; Chan, C. B.; Lowell, B. B. Uncoupling Protein-2 Negatively Regulates Insulin Secretion and Is a Major Link between Obesity, Î¸ Cell Dysfunction, and Type 2 Diabetes. *Cell* **2001**, *105* (6), 745–755.

(18) Fleury, C.; Neverova, M.; Collins, S.; Raimbault, S.; Champigny, O.; Levi-Meyrueis, C.; Bouillaud, F.; Seldin, M. F.; Surwit, R. S.; Ricquier, D.; Warden, C. H. Uncoupling Protein-2: A Novel Gene Linked to Obesity and Hyperinsulinemia. *Nat. Genet.* **1997**, *15* (3), 269–272.

(19) Mattiasson, G.; Shamloo, M.; Gido, G.; Mathi, K.; Tomasevic, G.; Yi, S.; Warden, C. H.; Castilho, R. F.; Melcher, T.; Gonzalez-Zulueta, M.; Nikolich, K.; Wieloch, T. Uncoupling Protein-2 Prevents Neuronal Death and Diminishes Brain Dysfunction after Stroke and Brain Trauma. *Nat. Med.* **2003**, *9* (8), 1062–1068.

(20) Valko, M.; Leibfritz, D.; Moncol, J.; Cronin, M. T. D.; Mazur, M.; Telser, J. Free Radicals and Antioxidants in Normal Physiological Functions and Human Disease. *Int. J. Biochem. Cell Biol.* **2007**, *39* (1), 44–84.

(21) Siems, W.; Grune, T. Intracellular Metabolism of 4-Hydroxynonenal. *Mol. Aspects Med.* **2003**, *24* (4–5), 167–175.

(22) Alary, J.; Gueraud, F.; Cravedi, J. P. Fate of 4-Hydroxynonenal in Vivo: Disposition and Metabolic Pathways. *Mol. Aspects Med.* **2003**, *24* (4–5), 177–187.

(23) Bacot, S.; Bernoud-Hubac, N.; Baddas, N.; Chantegrel, B.; Deshayes, C.; Doutheau, A.; Lagarde, M.; Guichardant, M. Covalent Binding of Hydroxy-Alkenals 4-HDDE, 4-HHE, and 4-HNE to Ethanolamine Phospholipid Subclasses. *J. Lipid Res.* **2003**, *44* (5), 917–926.

(24) Guichardant, M.; Taibi-Tronche, P.; Fay, L. B.; Lagarde, M. Covalent Modifications of Aminophospholipids by 4-Hydroxynonenal. *Free Radic. Biol. Med.* **1998**, *25* (9), 1049–1056.

(25) Seoane Fernandez, A.; Brea, R. J.; Fuertes, A.; Podolsky, K.; Devaraj, N. K. Biomimetic

Generation and Remodeling of Phospholipid Membranes by Dynamic Imine Chemistry. *J. Am. Chem. Soc.* **2018**, *140* (27), 8388–8391.

(26) Galeša, K.; Bren, U.; Kranjc, A.; Mavri, J. Carcinogenicity of Acrylamide: A Computational Study. *J. Agric. Food Chem.* **2008**, *56* (18), 8720–8727.

(27) Lajovic, A.; Nagy, L. D.; Guengerich, F. P.; Bren, U. Carcinogenesis of Urethane: Simulation versus Experiment. *Chem. Res. Toxicol.* **2015**, *28* (4), 691–701.

(28) Jovanović, O.; Pashkovskaya, A. A.; Annibal, A.; Vazdar, M.; Burchardt, N.; Sansone, A.; Gille, L.; Fedorova, M.; Ferreri, C.; Pohl, E. E. The Molecular Mechanism behind Reactive Aldehyde Action on Transmembrane Translocations of Proton and Potassium Ions. *Free Radic. Biol. Med.* **2015**, *89*, 1067–1076.

(29) Vazdar, K.; Vojta, D.; Margetić, D.; Vazdar, M. Reaction Mechanism of Covalent Modification of Phosphatidylethanolamine Lipids by Reactive Aldehydes 4-Hydroxy-2-Nonenal and 4-Oxo-2-Nonenal. *Chem. Res. Toxicol.* **2017**, *30* (3), 840–850.

(30) Sayre, L. M.; Lin, D.; Yuan, Q.; Zhu, X.; Tang, X. Protein Adducts Generated from Products of Lipid Oxidation: Focus on HNE and ONE. *Drug Metab. Rev.* **2006**, *38* (4), 651–675.

(31) Nadkarni, D. V; Sayre, L. M. Structural Definition of Early Lysine and Histidine Adduction Chemistry of 4-Hydroxynonenal. *Chem. Res. Toxicol* **1996**, *8*, 284–291.

(32) Sayre, L. M.; Arora, P. K.; Iyer, R. S.; Salomon, R. G. Pyrrole Formation from 4-Hydroxynonenal and Primary Amines. *Chem. Res. Toxicol.* **1993**, *6* (1), 19–22.

(33) Baker, A.; Žídek, L.; Wiesler, D.; Chmelík, J.; Pagel, M.; Novotny, M. V. Reaction of N-Acetylglycyllysine Methyl Ester with 2-Alkenals: An Alternative Model for Covalent Modification of Proteins. *Chem. Res. Toxicol.* **1998**, *11* (7), 730–740.

(34) Furuhata, A.; Ishii, T.; Kumazawa, S.; Yamada, T.; Nakayama, T.; Uchida, K. Nε-(3-Methylpyridinium)Lysine, a Major Antigenic Adduct Generated in Acrolein-Modified Protein. *J. Biol. Chem.* **2003**, *278* (49), 48658–48665.

(35) Globisch, M.; Kaden, D.; Henle, T. 4-Hydroxy-2-Nonenal (4-HNE) and Its Lipation Product 2-Pentylpyrrole Lysine (2-PPL) in Peanuts. *J. Agric. Food Chem.* **2015**, *63* (21), 5273–5281.

(36) Globisch, M.; Deuber, M.; Henle, T. Identification and Quantitation of the Lipation Product 2-Amino-6-(3-Methylpyridin-1-Ium-1-Yl)Hexanoic Acid (MP-Lysine) in Peanuts. *J. Agric.*

Food Chem. **2016**, *64* (34), 6605–6612.

(37) Kavianinia, I.; Yang, S.-H.; Kaur, H.; Harris, P. W. R.; Dobson, R. C. J.; Fairbanks, A. J.; Brimble, M. A. Synthesis and Incorporation of an Advanced Lipid Peroxidation End-Product Building Block into Collagen Mimetic Peptides. *Chem. Commun.* **2017**, *53* (60), 8459–8462.

(38) Becklin, R. R.; Desiderio, D. M. The Amount of Ultraviolet Absorbance in a Synthetic Peptide Is Directly Proportional to Its Number of Peptide Bonds. *Anal. Lett.* **1995**, *28* (12), 2175–2190.

(39) Ding, Y.; Cui, Y.; Li, T. New Views on the Reaction of Primary Amine and Aldehyde from DFT Study. *J. Phys. Chem. A* **2015**, *119* (18), 4252–4260.

(40) Doorn, J. A.; Petersen, D. R. Covalent Modification of Amino Acid Nucleophiles by the Lipid Peroxidation Products 4-Hydroxy-2-Nonenal and 4-Oxo-2-Nonenal. *Chem. Res. Toxicol.* **2002**, *15* (11), 1445–1450.

(41) Truhlar, D. G.; Garrett, B. C.; Klippenstein, S. J. Current Status of Transition-State Theory. *J. Phys. Chem.* **1996**, *100* (31), 12771–12800.

(42) Nozaki, K. Cis-Trans Isomerizations. II. The Mechanism of the Amine Catalyzed Isomerization of Diethyl Maleate. *J. Am. Chem. Soc.* **1941**, *63* (10), 2681–2683.

(43) Dugave, C.; Demange, L. Cis-Trans Isomerization of Organic Molecules and Biomolecules: Implications and Applications. *Chemical Reviews*. 2003, pp 2475–2532.

(44) Amarnath, V.; Valentine, W. M.; Amarnath, K.; Eng, M. A.; Graham, D. G. The Mechanism of Nucleophilic Substitution of Alkylpyrroles in the Presence of Oxygen. *Chem. Res. Toxicol.* **1994**, *7* (1), 56–61.

(45) Zhu, M.; Spink, D. C.; Yan, B.; Bank, S.; DeCaprio, A. P. Formation and Structure of Cross-Linking and Monomeric Pyrrole Autoxidation Products in 2,5-Hexanedione-Treated Amino Acids, Peptides, and Protein. *Chem. Res. Toxicol.* **1994**, *7* (4), 551–558.

(46) Lindahl, E.; Sansom, M. S. Membrane Proteins: Molecular Dynamics Simulations. *Current Opinion in Structural Biology*. 2008, pp 425–431.

(47) Pogozheva, I. D.; Mosberg, H. I.; Lomize, A. L. Life at the Border: Adaptation of Proteins to Anisotropic Membrane Environment. *Protein Science*. 2014, pp 1165–1196.

(48) Brown, M. F. Soft Matter in Lipid–Protein Interactions. *Annu. Rev. Biophys.* **2017**, *46* (1),

379–410.

(49) Thickett, S. C.; Gilbert, R. G. Emulsion Polymerization: State of the Art in Kinetics and Mechanisms. *Polymer (Guildf).* **2007**, *48* (24), 6965–6991.

(50) Pavlin, M.; Repič, M.; Vianello, R.; Mavri, J. The Chemistry of Neurodegeneration: Kinetic Data and Their Implications. *Mol. Neurobiol.* **2016**, *53* (5), 3400–3415.

(51) Warshel, A.; Parson, W. W. *Dynamics of Biochemical and Biophysical Reactions: Insight from Computer Simulations.*; 2001; Vol. 34.

(52) Warshel, A. Computer Simulations of Enzyme Catalysis: Methods, Progress, and Insights. *Annu. Rev. Biophys. Biomol. Struct.* **2003**, *32* (1), 425–443.

(53) Soulère, L.; Queneau, Y.; Doutheau, A. An Expeditious Synthesis of 4-Hydroxy-2E-Nonenal (4-HNE), Its Dimethyl Acetal and of Related Compounds. *Chem. Phys. Lipids* **2007**, *150* (2), 239–243.

(54) Zimmermann, L.; Moldzio, R.; Vazdar, K.; Krewenka, C.; Pohl, E. E. Nutrient Deprivation in Neuroblastoma Cells Alters 4-Hydroxynonenal-Induced Stress Response. *Oncotarget* **2017**, *8* (5), 8173–8188.

(55) Naidenova, N. M.; Arsatyants, R. A. Synthesis of N-Methylamides of N-Alpha-Acetylated Oligolysines. *Chem. Nat. Compd.* **1974**, *10* (4), 508–511.

(56) Marenich, A. V; Cramer, C. J.; Truhlar, D. G. Universal Solvation Model Based on Solute Electron Density and on a Continuum Model of the Solvent Defined by the Bulk Dielectric Constant and Atomic Surface Tensions. *J. Phys. Chem. B* **2009**, *113* (18), 6378–6396.

(57) Tomasi, J.; Mennucci, B.; Cammi, R. Quantum Mechanical Continuum Solvation Models. *Chem. Rev.* **2005**, *105* (8), 2999–3094.

(58) Plata, R. E.; Singleton, D. A. A Case Study of the Mechanism of Alcohol-Mediated Morita Baylis–Hillman Reactions. The Importance of Experimental Observations. *J. Am. Chem. Soc.* **2015**, *137* (11), 3811–3826.

(59) Becke, A. D. Density-functional Thermochemistry. III. The Role of Exact Exchange. *J. Chem. Phys.* **1993**, *98* (7), 5648–5652.

(60) Stephens, P. J.; Devlin, F. J.; Chabalowski, C. F.; Frisch, M. J. Ab Initio Calculation of Vibrational Absorption and Circular Dichroism Spectra Using Density Functional Force

Fields. *J. Phys. Chem.* **1994**, *98* (45), 11623–11627.

(61) Hehre, W. J.; Ditchfield, K.; Pople, J. A. Self-Consistent Molecular Orbital Methods. XII. Further Extensions of Gaussian-Type Basis Sets for Use in Molecular Orbital Studies of Organic Molecules. *J. Chem. Phys.* **1972**, *56* (5), 2257–2261.

(62) Hariharan, P. C.; Pople, J. A. The Influence of Polarization Functions on Molecular Orbital Hydrogenation Energies. *Theor. Chim. Acta* **1973**, *28* (3), 213–222.

(63) Fukui, K. The Path of Chemical Reactions - the IRC Approach. *Acc. Chem. Res.* **1981**, *14* (12), 363–368.

(64) Frisch, M. J.; Trucks, G. W.; Schlegel, H. B.; Scuseria, G. E.; Robb, M. A.; Cheeseman, J. R.; Scalmani, G.; Barone, V.; Mennucci, B.; Petersson, G. A.; Nakatsuji, H.; Caricato, M.; Li, X.; Hratchian, H. P.; Izmaylov, A. F.; Bloino, J.; Zheng, G.; Sonnenberg, J. L.; Hada, M.; Ehara, M.; Toyota, K.; Fukuda, R.; Hasegawa, J.; Ishida, M.; Nakajima, T.; Honda, Y.; Kitao, O.; Nakai, H.; Vreven, T.; Montgomery Jr., J. A.; Peralta, J. E.; Ogliaro, F.; Bearpark, M. J.; Heyd, J.; Brothers, E. N.; Kudin, K. N.; Staroverov, V. N.; Kobayashi, R.; Normand, J.; Raghavachari, K.; Rendell, A. P.; Burant, J. C.; Iyengar, S. S.; Tomasi, J.; Cossi, M.; Rega, N.; Millam, N. J.; Klene, M.; Knox, J. E.; Cross, J. B.; Bakken, V.; Adamo, C.; Jaramillo, J.; Gomperts, R.; Stratmann, R. E.; Yazyev, O.; Austin, A. J.; Cammi, R.; Pomelli, C.; Ochterski, J. W.; Martin, R. L.; Morokuma, K.; Zakrzewski, V. G.; Voth, G. A.; Salvador, P.; Dannenberg, J. J.; Dapprich, S.; Daniels, A. D.; Farkas, Ö.; Foresman, J. B.; Ortiz, J. V; Cioslowski, J.; Fox, D. J. Gaussian 09. Gaussian, Inc.: Wallingford, CT, USA 2009.

(65) Warshel, A. Calculations of Enzymatic Reactions: Calculations of PKa, Proton Transfer Reactions, and General Acid Catalysis Reactions in Enzymes. *Biochemistry* **1981**, *20* (11), 3167–3177.